JOURNAL OF Applied Polymer SCIENCE

Photoactive Behavior of Polyacrylonitrile Fibers Based on Silver and Zirconium Co-Doped Titania Nanocomposites: Synthesis, Characterization, and Comparative Study of Solid-Phase Photocatalytic Self-Cleaning

Hadi Fallah Moafi, Abdollah Fallah Shojaie, Mohammad Ali Zanjanchi
Department of Chemistry, Faculty of Science, University of Guilan, Rasht, Iran
Correspondence to: H. F. Moafi (E-mail: fallah.m@guilan.ac.ir)

ABSTRACT: Silver and zirconium co-doped and mono-doped titania nanocomposites were synthesized and deposited onto polyacrylonitrile fibers via sol–gel dip-coating method. The resulted coated-fibers were characterized by X-ray diffraction (XRD), scanning electron microscopy, energy dispersive spectroscopy, transmission electron microscopy, diffuse reflectance spectroscopy, thermogravimetric analysis, and BET surface area measurement. Photocatalytic activity of the TiO_2-coated and TiO_2-doped coated fibers were determined by photomineralization of methylene blue and Eosin Y under UV–vis light. The progress of photodegradation of dyes was monitored by diffuse reflectance spectroscopy. The XRD results of samples indicate that the TiO_2, Ag-TiO_2, Zr-TiO_2, and Ag-Zr-TiO_2 consist of anatase phase. All samples demonstrated photo-assisted self-cleaning properties when exposed to UV–vis irradiation. Evaluated by decomposing dyes, photocatalytic activity of Ag–Zr co-doped TiO_2 coated fiber was obviously higher than that of pure TiO_2 and mono-doped TiO_2. Our results showed that the synergistic action between the silver and zirconium species in the Ag-Zr TiO_2 nanocomposite is due to both the structural and electronic properties of the photoactive anatase phase. These results clearly indicate that modification of semiconductor photocatalyst by co-doping process is an effective method for increasing the photocatalytic activity. © 2012 Wiley Periodicals, Inc. J. Appl. Polym. Sci. 000: 000–000, 2012

KEYWORDS: titania nanocomposite; Ag–Zr co-doped; self-cleaning; polyacrylonitrile fibers; sol–gel; methylene blue; Eosin Y

Received 9 October 2011; accepted 7 March 2012; published online 00 Month 2012
DOI: 10.1002/app.37664

INTRODUCTION

Metal oxide semiconductor photocatalysts have attracted widespread interest for potential application in photocatalytic degradation of environmental organic pollutants.[1–3] Among the photocatalysts that have been examined, nanocrystalline TiO_2 was considered a very promising photocatalyst for pollutant photodegradation owing to its remarkable features including high photocatalytic activity, inexpensive, nontoxicity, and good physicochemical stability.[4,5] Unfortunately, TiO_2 exhibits photoactivity only under ultraviolet light excitation because of its wide bandgap (3.2 eV), which means that only about 3–5% of arriving solar energy on the Earth's surface can be utilized. Furthermore, TiO_2 presents a relatively high electron–hole recombination rate which is unfavorable to its photoactivity. Therefore, it is particularly important to extend the photoactivity of TiO_2 to visible light region and inhibit the recombination of photogenerated electrons and holes. To improve the visible photoactivity of TiO_2, one method is to control structure of TiO_2 particles such as the surface area, crystal phase, crystallite size, and morphology of particles. The other method is to modify TiO_2 particles, involving metal or nonmetal ions doping,[6–15] dye sensitization,[4,16,17] semiconductor coupling,[18] and deposition of noble metals.[19–22] Among various modification methods to TiO_2, doping of TiO_2 with metal or nonmetal has been widely investigated. Nonmetal doping could obviously shift the light absorption threshold to visible light range. However, the content of doped nonmetal component would decrease during annealing process; thus, the visible photoactivity of TiO_2 would decrease. Fortunately, doping of TiO_2 with metal ions could also significantly enhance its visible photoactivity. The doped metal ions could enhance the quantum efficiency via inhibiting the recombination of photogenerated electrons and holes, by acting as electron traps; expand the light absorption range and improve the redox potential of the

photogenerated radicals. Additionally, the doped metal components would not be lost during annealing process. Therefore, transition metal doped TiO_2 have been significantly investigated for their high photocatalytic activities under irradiation of UV and visible light. Alternatively, noble metal-modified TiO_2 nanoparticles[19,20] could effectively eliminate the recombination of electron–hole pairs to enhance the photoactivity and simultaneously extend their wavelength response towards the visible light area.

Currently, some investigators devoted themselves to improve the photoactivity of TiO_2 through co-doping process.[23–33] These studies demonstrated that the observed high photocatalytic activity of the samples could be ascribed to a synergetic effect between doping ions. These reports indicated that modification of titania by co-doping may be an effective method for increasing the photocatalytic activity.

One of the most significant applications of photocatalysis processes is the development of self-cleaning materials. These self-cleaning materials provide promising applications in automobile windshields, windows of high-rise buildings, and other fields utilized for sterilization, deodorization, antifog, and room air cleaning. Recently, several studies have been reported the promising potentials of nontoxic and inexpensive TiO_2 nanoparticles for imparting multifunctional properties to different textile materials.[34–50] The compatibility of TiO_2 nanoparticles surface with fiber surface chemical functionalities is one of the most important prerequisites for obtaining stable composite system and long-term durability effects.

In the view point of practical application, it is very important to immobilize the fine TiO_2 particles onto suitable substrates in order to create self-cleaning application. The fabrication method accompanied with high temperature such as chemical vapor deposition (CVD), anodization, and thermal oxidation of Ti metal, ultrasonic nebulization, and pyrolysis, would bring about the cracking and/or peeling of the TiO_2 film because of the shrinkage during the crystallization of deposited amorphous films. Furthermore, the heating process precludes the production of TiO_2 film on substrates with low thermal stability such as polymers.[51] In order to overcome these drawbacks involved in the high temperature process, low-temperature route to nanocrystalline TiO_2 particles or thin films based on sol–gel process have been reported.[35,40,43,46,47,49,50]

In this work, we report the route that we developed as a facile and effective method to create self-cleaning coatings based on titania nanocomposites on polyacrylonitrile (PAN) fibers. The silver, zirconium, and silver-zirconium doped titania were prepared using the sol–gel method at ambient temperature on surface of fibers. The photocatalytic performance of the coated-fibers with these materials was investigated following their characterization.

It is well known that PAN fibers has been widely used in many industries because of their desirable properties like abrasion resistance, thermal and mechanical stability, high tensile strength, good resilient, and tolerance to most solvents.

EXPERIMENTAL

Reagents and Materials

Titanium tetraisopropoxide (TIP), acetic acid, zirconium (IV) acetylacetonate, silver nitrate, methylene blue, and Eosin Y were purchased from Merck (Germany) and was of analytical reagent grade and used without further purification. Deionized water was used in all experimental preparations. The used PAN fibers were 100% woven fabric, plain construction, with a density of 180 g m^{-2}. The PAN fibers were scoured with detergent to remove wax, grease, and other chemical residues from fabrics before coating. For this purpose, the PAN fibers were washed first by water and detergent at 80°C for 30 min to remove the impurities and then washed several times by a large amount of deionized water. They were further cleaned in acetone (Merck) for 60 min and dried at room temperature for 24 h.

Synthesis Procedure

The sol–gel method was used for the preparation of doped and co-doped TiO_2 nanocrystals. Titanium isopropoxide (TIP) was used as the precursor for titania sol preparation. Four different sols, pure TiO_2, Ag-doped TiO_2, Zr-doped TiO_2, and Ag–Zr co-doped TiO_2 sols, were prepared by sol–gel method at low temperature. In a typical synthesis, 10 mL of TIP was added to acetic acid (20 mL) with stirring. Deionized water (60 mL) was added to the mixture dropwise with vigorous stirring. TIP, acetic acid, and water are in 1 : 10 : 100 molar ratios. The solution was stirred for 2 h to get a clear transparent sol. To prepare the doped and the co-doped titania sols, the above procedure was repeated. For synthesis of Ag-TiO_2, a certain amount of silver nitrate (2 mol % with respect to TIP) was dissolved in deionized water (60 mL), stirred and then was added into the mixture of TIP and acetic acid dropwise with vigorous stirring. For preparation of Zr-TiO_2, the required amount of zirconium (IV) acetylacetonate (2 mol % with respect to TIP) was treated the same way as described for Ag-TiO_2. These solutions were stirred for 2 h to get a clear transparent doped titania sol. In the synthesis procedure of Ag–Zr co-doped titania sol, 2 mol % of silver nitrate with respect to TIP and 2 mol% of zirconium (IV) acetylacetonate with respect to TIP were dissolved into deionized water under vigorous stirring and then the solution was added into the mixture of TIP and acetic acid dropwise while stirring rapidly at room temperature. The obtained co-doped sol was then stirred for 2 h to get a clear transparent sol and ready for dip-coating procedure.

Coating Processes

The dip-pad-dry-cure process was employed to apply the as-prepared sols onto the fibers for preparing a durable layer. The cleaned substrates were dipped in the as-prepared sols for 5 min and then padded with a padder. The padded substrates were air-dried for 30 min at 100°C and finally cured at 150°C for 15 min in a preheated curing oven to ensure particles adhesion to the substrate surface. Finally, the impregnated fibers were rinsed in deionized water. During this step, the unattached particles were removed from the fiber surface.

Photocatalytic Test

The photocatalytic activity of our coated-fibers was examined by exposing the samples containing preadsorbed methylene blue (MB) and Eosin Y to UV–vis light. For this purpose, 100 mL aqueous solutions (1.0×10^{-5} molL^{-1}) of MB and Eosin Y were prepared. Both bare and coated fibers are treated in MB and Eosin Y solutions. The same amount of each sample was immersed under mild stirring in the same volume of the solution and remained overnight to complete the adsorption. For each of the samples (pure and coated fabrics), a piece of PAN fabric with 2×2 cm^2 dimensions were used for soaking in the dyes solution. The fibers were drawn out of the dyes solution and dried at room temperature. The so-obtained samples could be fixed in the front of the integrating sphere hole of the diffuse reflectance attachment. The amount of coated TiO_2 may be obtained from thermogravimetric (TG) data. According to our TG analysis it was estimated to be about 11.5% for the TiO_2-coated sample. These selected samples were exposed to UV–vis light to test their photoactivity. The similar settings were performed in several intervals times during the test. For photocatalytic reactions, the irradiation was carried out on dry samples, by means of a high-pressure mercury lamp (HPMV 400 W, Germany). The lamp yields a spectrum ranging from ultraviolet to visible light (200–800 nm). Details of the experimental procedure were described in our previous work.[35–38]

The photocatalytic decomposition was determined from the following equation.

$$\text{Photocatalytic decomposition} = (C_0 - C)/C_0 = (A_0 - A)/A_0$$

where, C_0 represents the initial concentration of the dyes on fiber surface, C the final concentration after illumination by light, A_0 the initial absorbance, and A the variable absorbance.

Characterization Techniques

To investigate the morphology of the pure and coated fibers, scanning electron microscopy (SEM) images were obtained on a Philips, XL30 equipped with an energy dispersive (EDS) micro-analysis system for compositional analysis of the TiO_2-coated fibers. For the SEM and EDS analysis, samples were covered with Au. The particles sizes were obtained by transmission electron microscope (TEM) images on a Philips CM10 instrument with an accelerating voltage of 100 kV. For photodecomposition reaction, the UV–vis reflectance spectra were recorded at room temperature by a UV-2100 Shimadzu spectrophotometer in the reflectance mode by investigating the evolution of the absorbance. The BET specific surface area of the synthesized nanoparticles was determined by nitrogen adsorption at liquid nitrogen temperature on a Sibata SA-1100 surface area analyzer. X-ray diffraction measurements were recorded by a D8 Bruker Advanced diffractometer with Cu-Kα radiation, scan rate 0.02 2θ/s and within a range of 2θ of 10–70 degree at room temperature. To investigate the amounts of TiO_2 and TiO_2 nanocomposites deposited on the fibers and also thermal behavior of samples, thermogravimetric analysis was performed in air flow (ramp of 10°C min^{-1}) by Thermogravimetric analyzer (TGA V5.1A DuPont 2000).

RESULTS AND DISCUSSION

XRD Analysis

The X-ray diffraction (XRD) patterns of pure, coated-fibers, and sol-derived powders are reported in Figures 1 and 2. Figure 1 (peak a) shows two peaks: the intense one at 17° and the broad one at 29°, which constitute the typical XRD pattern of PAN fibers.[52] The strong peak at $2\theta = 17°$ corresponds to 100 reflection of the crystalline structure of the PAN fiber.[53] Figure 1b to 1e shows the XRD patterns of TiO_2-coated and the TiO_2-doped/coated fibers. Since the amount of TiO_2 was low on the fibers surface, therefore, there is a low intensity for the characteristics reflections of TiO_2 phase in the XRD patterns. The reflections observed at $2\theta = 25°$, 37°, and 55° are related to anatase phase.

Figure 2 shows the XRD patterns of sol–gel derived TiO_2, Ag-doped TiO_2, Zr-doped TiO_2, and Ag–Zr co-doped TiO_2 powders. As it is evident from the diffractograms, all the reflections belong to pure anatase phase and no additional reflections belonging to other phases are observed. These observations indicate that there is virtually no phase change in TiO_2 structure in the process of doping or co-doping. There were no detectable peaks relating to the presence of a separate dopant metal phase in any corresponding pattern. This could be attributed to the fact that the dopant metals/metal oxides were too low in concentration to be seen as a separate phase or they have been distributed within the lattice of TiO_2 which in this case only reflections of TiO_2 anatase phase are observed in the XRD patterns. The relatively high width of the reflections associated with the TiO_2 phase suggests that the size of the particles is quite small. It is observed that doping of Ag and Zr reduced the grain size and enlarged the surface areas of nanoparticles. The average grain size are calculated using the Scherrer's equation based on the fullwidth at half-maximum (FWHM) of the (101) peak of the compounds. The crystallite size, on the other hand, have been reduced with the doping as indicated by the peak broadening in the XRD patterns of Ag-TiO_2 and Zr-TiO_2 (Table II).

The phase structure, crystallite size, and crystallinity of TiO_2 play an important role in photocatalytic activity. Many studies have confirmed that the anatase phase of titania shows higher photocatalytic activity than the brookite or rutile phases.[54] From the wide angle XRD patterns (Figure 2), the titania and titania nanocomposites exist only in anatase phase. The samples did not show any change of anatase phase prior and after using dopants. This illustrates that doping and co-doping process did not change the catalysts structure or its crystallinity. The smaller crystallite size indicates that the preparation method used in the present work can effectively prompt the crystallization and inhibit the grain growth.

Our nano TiO_2 and the doped nano TiO_2 were prepared in the presence of acetic acid. This is due to the fact that protonation of TiO_2 nanoparticles can prevent further crystallization. In addition, the excess acetate anion adsorbed on the surface of

Applied Polymer SCIENCE

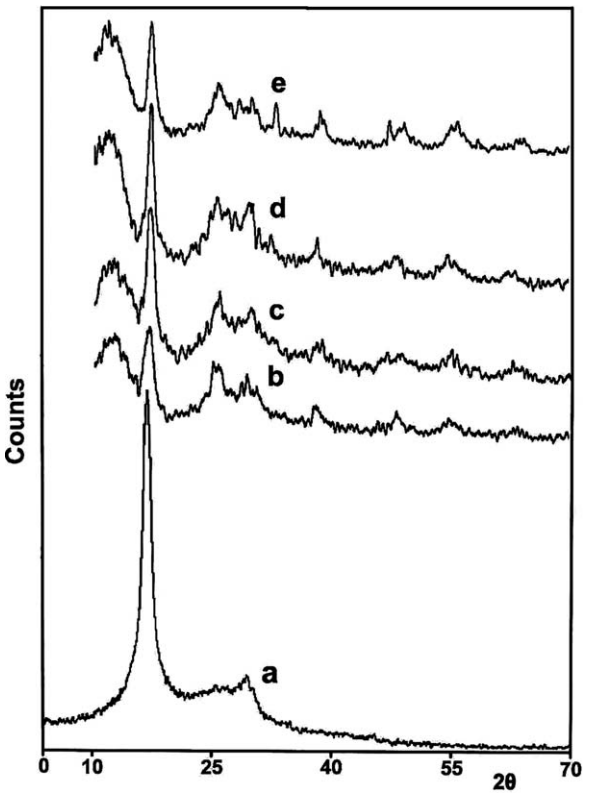

Figure 1. XRD patterns of: (a) pure PAN fiber, (b) TiO_2 coated fiber, (c) Ag-TiO_2 coated fiber, (d) Zr-doped TiO_2 coated fiber, and (e) Ag-Zr-TiO_2 coated fiber.

TiO_2 could also suppress the growth of nano TiO_2. This role of acetate anion on the surface of TiO_2 could be responsible for the decrease in the crystallite size of TiO_2 during the sol–gel synthesis.[13]

Figure 2 displays that characteristic peaks broadened when the ions doped into TiO_2. The ionic radius of the dopant ion is important factor, which can strongly influence the ability of the dopant to enter into TiO_2 crystal lattice. If the ionic radius of the doping metal ions matches those of the lattice metal ion in oxides, the doping metal ion will substitute itself for the lattice in the doping reactive process (substitutional mode). Whereas, the ions with the radius which are much bigger or smaller than that of Ti^{4+} cause crystal lattice distortion.[55]

The ionic radius of Ag^{+} (0.115 nm) is bigger than that of Ti^{4+} (0.068 nm). Therefore, it is difficult for Ag^{+} to really enter into the lattice of TiO_2. However, the electronegativity and the ionic radius of Zr^{4+} ion (1.2, 0.072 nm, respectively) are closer to Ti^{4+} ion, it is expected Zr^{4+} ions will replace lattice Ti^{4+} ions and thus occupy lattice Ti^{4+} positions. In doping process, the lattice structure of TiO_2 is locally distorted by incorporation of Zr^{4+} ion dopant into TiO_2. To clarify the effect of these dopants on the lattice structure of TiO_2, the lattice parameters (*a*, *b*, and *c*, in anatase form, $a = b \neq c$) of the catalysts were measured using Bragg's law and a formula for a tetragonal system:

Table I. Lattice Parameters of TiO_2 and TiO_2 Nanocomposites

	Lattice parameters (Å)	
Catalysts	$a = b$	C
Undoped TiO_2	3.785	9.352
Ag-TiO_2	3.779	9.365
Zr-TiO_2	3.781	9.518
Ag-Zr-TiO_2	3.782	9.456

$$\text{Bragg's law} : 2d\sin\theta = \lambda$$

$$1/d^2 = h^2/a^2 + k^2/b^2 + l^2/c^2$$

where *d* is the crystal planes spacing, λ is the X-ray wavelength, θ is the diffraction angle of crystal plane, *h, k, l* are the crystal face indexes, and *a, b,* and *c* are lattice parameters.

The results are summarized in Table I. The table clearly shows that the lattice parameters of all TiO_2 samples remain almost unchanged along the *a* and *b* axes, whereas *c* axis parameter increases in Zr-TiO_2 and Ag-Zr-TiO_2 due to the presence of adventitious Zr^{4+} ion. Since ionic radius of Zr^{4+} (0.072 nm) as dopant is closer than Ti^{4+} (0.068 nm) in the TiO_2 structure, for possible diffusion of Zr^{4+} along the *c*-axis to substitute Ti^{4+} in TiO_2, the lattice parameters of *c* increase relative to that of TiO_2. Consequently, some structural defects such as oxygen vacancies might be generated on the surface of Zr-TiO_2 and Ag-Zr-TiO_2. Also, Table I shows that the lattice parameter *c* of Ag-TiO_2 does not change much compared to that of undoped TiO_2. This could be attributed to the Ag dopant which is merely

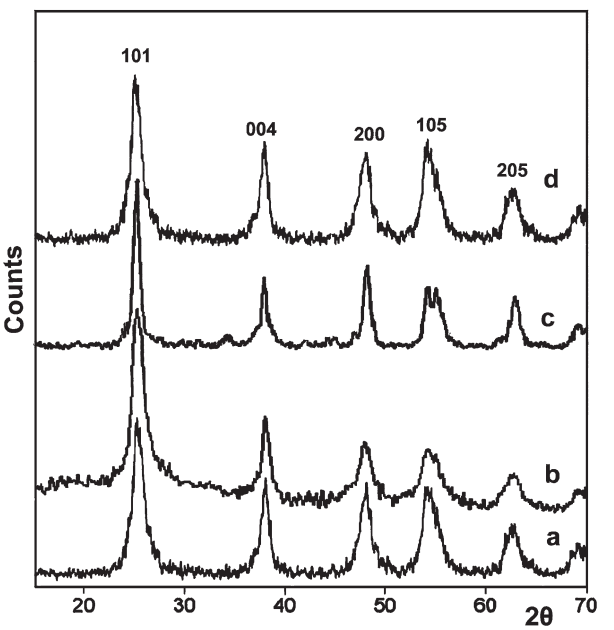

Figure 2. XRD patterns of sol-derived powders at low temperature: (a) TiO_2, (b) Ag-doped TiO_2, (c) Zr-doped TiO_2, and (d) Ag–Zr co-doped TiO_2.

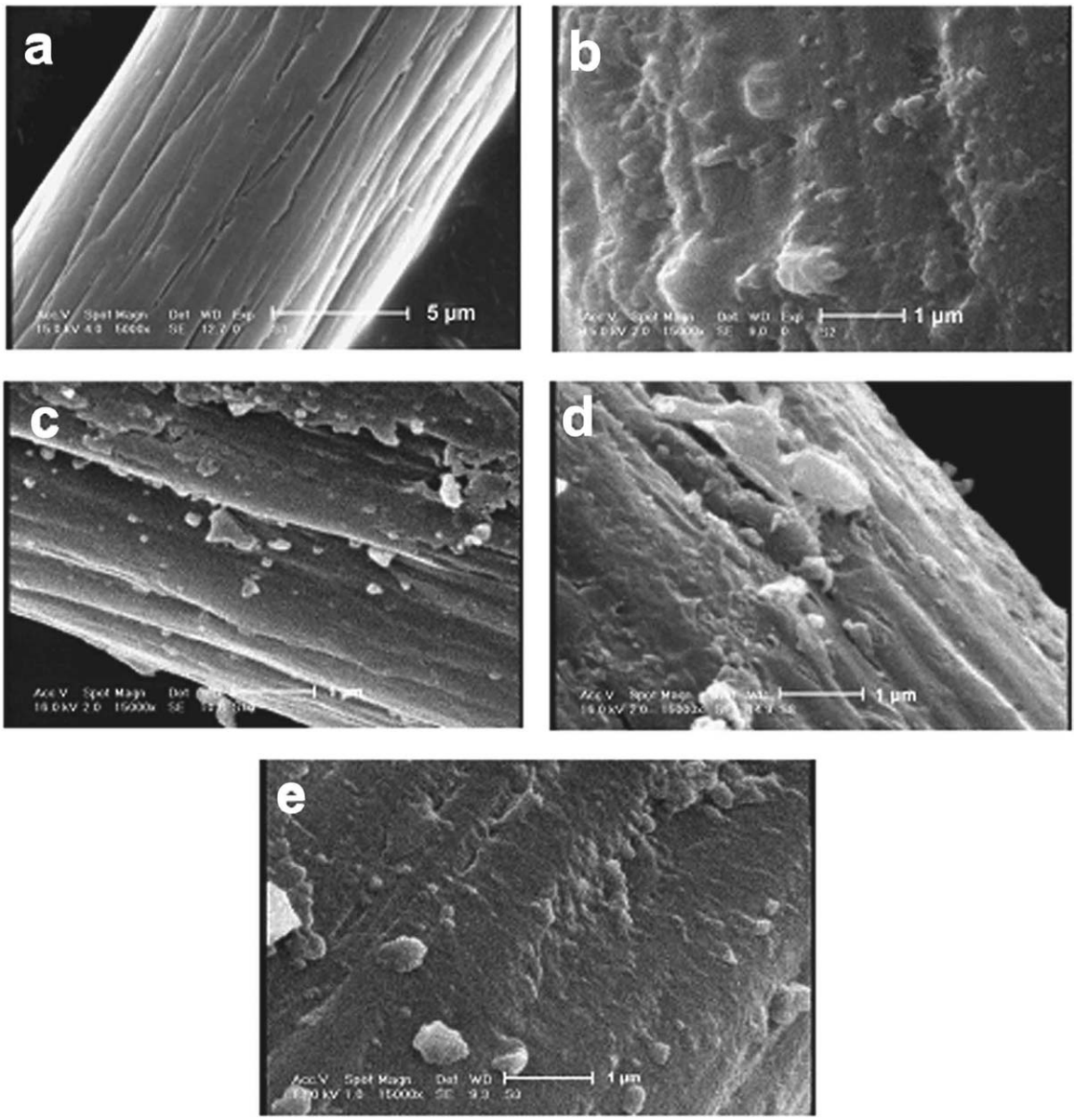

Figure 3. SEM images of: (a) pure fiber, (b) TiO_2-coated fiber, (c) Ag-TiO_2-coated fiber, (d) Zr-TiO_2 coated fiber, and (e) Ag-Zr-TiO_2-coated fiber.

placed on the surface of the crystals without being covalently anchored into the crystal lattice.

Morphological and Compositional Analysis

Surface morphology of the pure fibers and the fibers after coating with TiO_2 and doped TiO_2 was studied by SEM (Figure 3). Figure 3(a) shows the surface of the pristine fibers. The surface of the fibers is relatively smooth, and the groove-like structure on the PAN fibers surfaces seems clear. In contrast to that the micrograph of the treated fibers shows agglomerates of spherical particles deposited on its surface. However, Figure 3(b) shows that treated fibers with TiO_2 after being washed with deionized water are covered by continuous and homogeneous dispersed TiO_2 agglomerates. SEM images reveal that the most of them are irregularly shaped and relatively spherical with dimensions that are less than 100 nm [Figure 3(b)]. Figure 3(c) shows the treated fibers with Ag-TiO_2 nanosol after washing process. The Ag-TiO_2 coated-fibers show a surface morphology similar to that of the bare TiO_2 coating. It can be seen that the deposited nanoparticles were composed by agglomerates of fine particles with dimension of several tens nanometers and TiO_2 particles were uniformly distributed on the fiber surface. The SEM images of the treated samples with Zr-doped and Ag–Zr co-doped TiO_2 are shown in Figure 3(d, e). These figures indicate that shape of the particles are quite similar to each other and likely become spherical in general. Figure 4 shows the micrograph of the sol-derived TiO_2 and doped TiO_2 nanoparticles at 150°C. It is clear that the morphology of the powder nanoparticles is rather similar to the nanoparticles coated on the fiber surface. But the powder nanoparticles show more agglomerates than that of the coated nanocomposites.

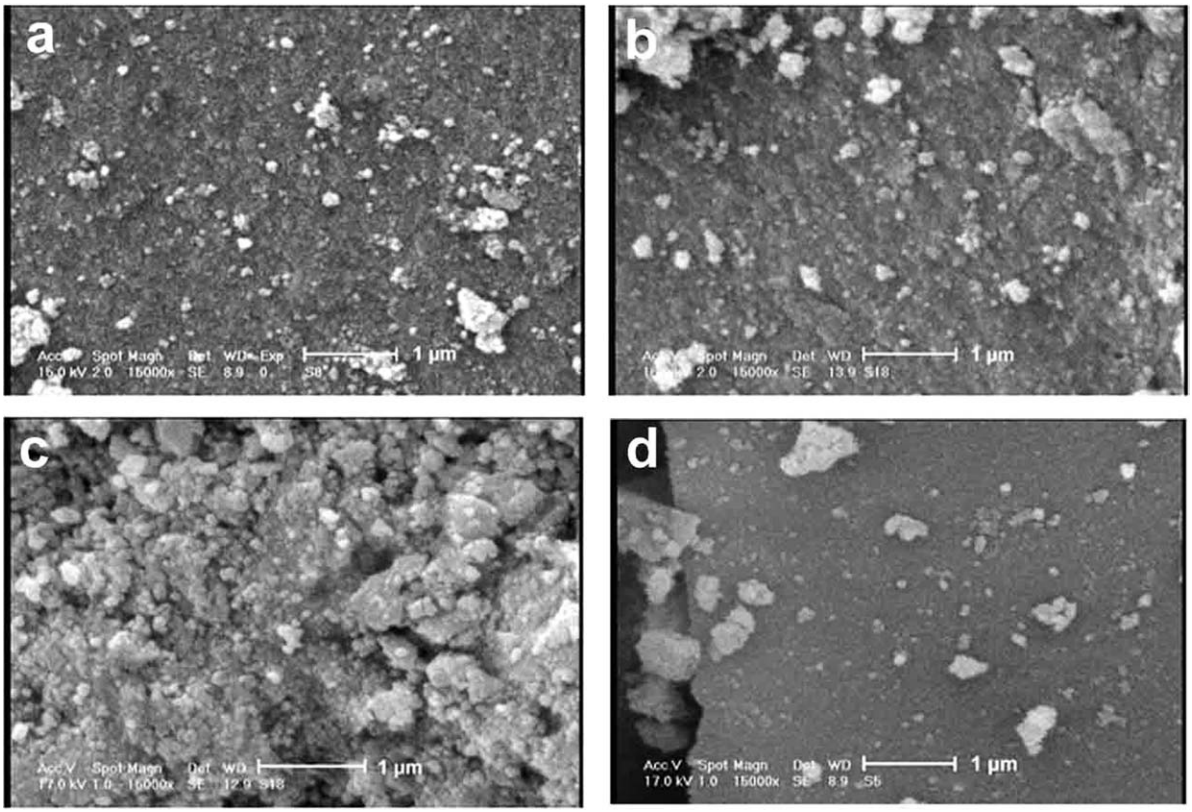

Figure 4. SEM images of sol-derived powders at 150°C: (a) TiO_2, (b) Ag-TiO_2, (c) Zr-TiO_2, and (d) Ag-Zr-TiO_2.

The elemental analysis of the treated samples by EDS analysis are shown in Figure 5. According to the analysis, the amount of Ti and other elements slightly varies, meaning that doping ions are occupied in the crystal structure. On the basis of this result, it is noteworthy to mention that after washing process, remarkable amount of TiO_2 and doping ions are still present on the fibers surface. This means that TiO_2 and TiO_2 nanocomposites have sufficient adhesion towards the fibers in order to resist a washing process. This observation indicates that the washing process can only remove the adsorptive grain under this condition.

Figure 6 depicts transmission electron micrographs of all samples. TEM image of TiO_2 on the coated fiber [Figure 6(a)] shows that the deposited titania consists of nanoclusters with average size of ~5 nm which is consistent with the XRD results. It is noticeable that the TiO_2 nanoclusters are distributed homogenously on the fiber surface. The TEM image of Ag-TiO_2 on the surface of the fiber shows that the size of Ag-TiO_2 particles are smaller than TiO_2, mostly less than 5 nm, as seen in Figure 6(b). For Ag-TiO_2 sample, Ag species are well dispersed on the TiO_2 nanoparticles and Ag particles have larger dimensions than that of TiO_2 nanoparticles. The size distributions of Ag nanoparticles indicate that the vast majority is in the 10–20 nm range. However, the small size of silver and TiO_2 nanoparticles suggests that the exposed surface area of Ag/TiO_2 coating is very large.

Figure 6(c) shows that Zr-doped TiO_2 sample consist of the agglomerates of primary particles with an irregular shape and size less than 5 nm which is in good agreement with XRD data. The shape of the Ag–Zr co-doped TiO_2 nanoparticles was observed as aggregated nanoparticles with average particle size of 5–10 nm [Figure 6(d)]. Indeed, it is demonstrated that Zr and Ag doping could inhibit the increase of TiO_2 particle size. Therefore, this result may be attributed to the presence of doping component in the TiO_2 framework. Indeed, the entry of Zr^{4+} and Ag^{+} in the TiO_2 lattices suppresses the particle growth. The formation of Ti—O—Zr or Ti—O—Ag inhibits the transition of TiO_2 phase and blocks the Ti—O species at the interface with TiO_2 domains stabilizing them, thus preventing the agglomeration of TiO_2 nanoparticles and thus preventing the rutile growth. The TEM image of co-doped sample shows that its particles size is slightly larger than that of other samples (5–10 nm). The reason can be attributed to the simultaneous presence of both Ag and Zr dopants which might increase agglomeration nanoparticles. This results in the increasing of particle size.

UV–Visible Diffuse Reflectance Spectra

UV–vis diffuse reflectance spectroscopy directly provides some insight into the interactions of the photocatalyst materials with photon energies. The reflectance spectra of TiO_2, Ag-doped TiO_2, Zr-doped TiO_2, and Ag–Zr co-doped TiO_2 are illustrated in Figure 7. For the sake of comparison spectrum of Degussa–TiO_2 (P25) was also included. The spectrum of TiO_2 consists of a single absorption usually ascribed to charge-transfer from the valence band (mainly formed by 2p orbitals of the oxide

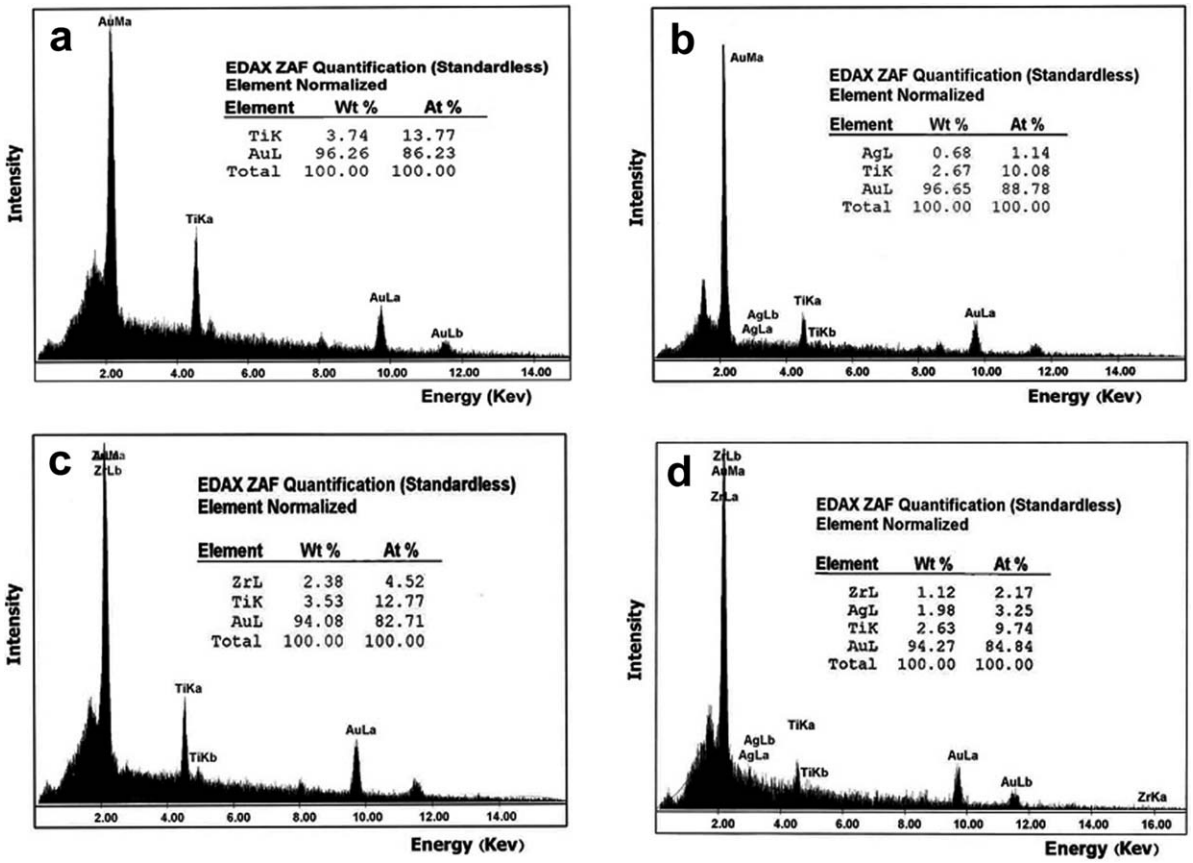

Figure 5. EDS analysis of: (a) TiO_2 coated fiber, (b) Ag-TiO_2 coated fiber, (c) Zr-TiO_2 coated fiber, and (d) Ag-Zr-TiO_2 coated fiber.

anions) to the conduction band (mainly formed by $3dt_2g$ orbitals of the Ti^{4+} cations).[19] We observed an inevidence shift of the optical absorption edge for the doped TiO_2 systems toward the visible regions. Surely, this shift towards the longer wavelengths originates from the band gap narrowing of titanium dioxide by incorporation of dopant ions. In the Ag-TiO_2 sample, addition of silver ions causes significant changes to the absorption spectrum of TiO_2 resulting in absorbance from 400 nm to entire visible region. The absorbance in the visible region for the Ag-TiO_2 system shows that lower energy transitions are possible. This is because the metal clusters give rise to localized energy levels in the band gap of TiO_2 into which valence band electrons of TiO_2 are excited at wavelength longer than 400 nm. The Zr-doped TiO_2 crystals exhibited absorptions that extended to longer wavelengths. Presumably, these red shifts and reduced band gaps resulted either from defects caused by trace amounts of Zr^{4+} in the TiO_2 lattice. The red shift and reduced band gap in Ag–Zr co-doped is higher than that of other samples. The band gap energy of the doped samples was determined from the equation, $E_g = 1239.8/\lambda$, where λ is the wavelength (nm) of the exciting light (Table II).

The difference in absorption edge wavelength for the nanocomposites coatings clearly indicates difference in the band gap of the samples. The doped and co-doped samples do not show a sharp absorption edges as observed for the undoped TiO_2. Instead, they have a long tails extending up to 700 nm. The tail absorption can be assigned to the formation of impurity species within the band gap of TiO_2. The electronic transitions between these impurities and the valence or conduction band effectively shift the band edge absorption to visible light region. It may also originate from defects associated with oxygen vacancies. The absorption edge of the Ag-TiO_2 is about 435 nm, the band gap is estimated to be 2.85 eV, while the edge of the absorption of the Zr-TiO_2 samples is shifted to approximately 425 nm, corresponding to a band gap energy of 2.91 eV. The co-doped Ag-Zr-TiO_2 exhibits the largest visible light absorption among the four samples. The absorption edge of the Ag-Zr-TiO_2 sample has shifted to about 450 nm, corresponding to band gap energy of 2.75 eV. While, the absorption onset for anatase TiO_2 coating is 400 nm, with band gap energy of 3.1 eV. The results indicate that the optical absorption of sample co-doped with Ag^+ and Zr^{4+} in the visible region is relatively stronger than the undoped sample and doped sample with Ag^+ or Zr^{4+} alone. So, the electronic property affect the anatase band gap and subsequently enhance the visible light photon absorption. Therefore, the best photocatalytic activity can be attained by Ag–Zr co-doped sample.

BET Surface Area Analysis

In general, the surface area of the catalyst is the most important factor influencing the photocatalytic activity. The surface area of nanoparticles was determined using the nitrogen gas adsorption method. Table II summarizes the BET surface areas

Applied Polymer SCIENCE

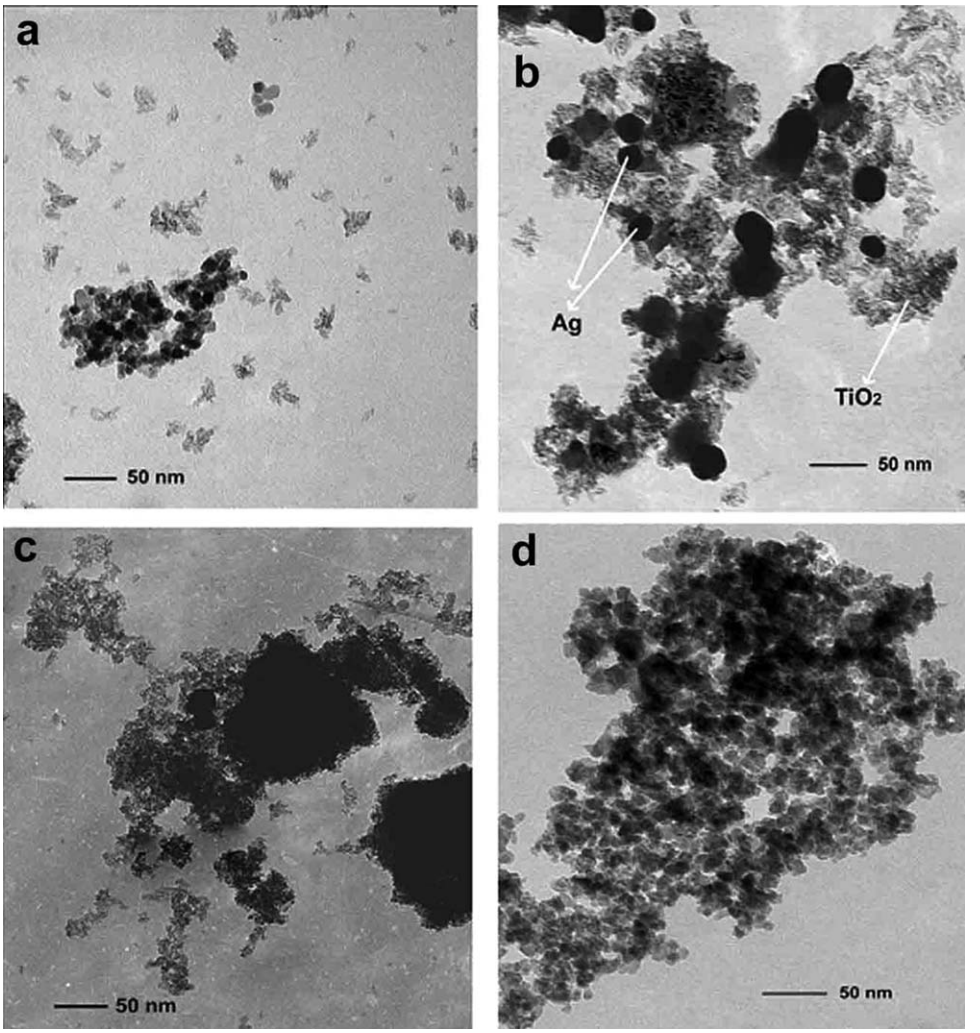

Figure 6. TEM images of: (a) TiO_2 on PAN fiber, (b) Ag-TiO_2 nanocomposite on fiber, (c) Zr-TiO_2 nanocomposite on fiber, and (d) Ag-Zr-TiO_2 nanocomposite on fiber.

and pore volumes of TiO_2, Ag-TiO_2, Zr-TiO_2, and Ag-Zr-TiO_2. It is obvious from the table that all the prepared samples have very high surface area compared to that of Degussa TiO_2 (P25). The doping by Ag^+ ion slightly increases surface area and pore volume of TiO_2, whereas, doping by Zr^{4+} and co-doping process decrease the surface area of Zr-TiO_2, and Ag-Zr-TiO_2. The BET surface area of the Zr-TiO_2 sample decreases to about 290 m^2/g, indicating that doping of Zr ion might result in the agglomeration of the nanoparticles, which is in agreement with the TEM result. Also, BET surface area of the co-doped sample is lower than that of the single doped samples. The reason can be attributed to the simultaneous presence of both Ag and Zr dopants which might increase agglomeration of nanoparticles. This observation confirms the possible mesoporous nature of the synthesized TiO_2 and TiO_2 nanocomposites.

Thermogravimetric Analysis

The TG analysis of the pure and treated fibers was carried out in air atmosphere at a heating rate of 10 °C min^{-1}. The weight

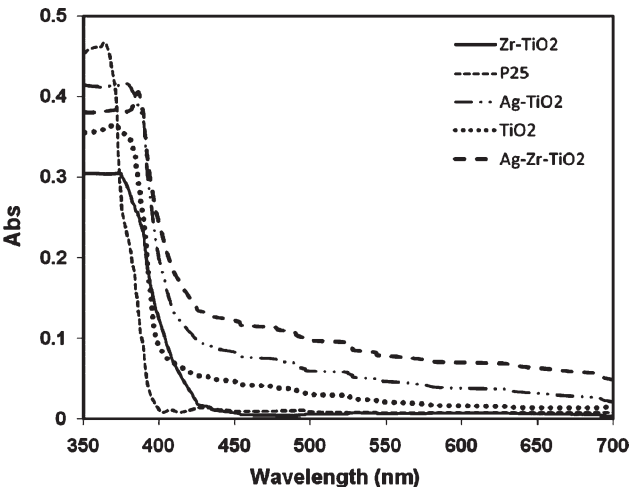

Figure 7. Diffuse reflectance spectra of synthesized TiO_2 nanoparticles and TiO_2 nanocomposites on PAN substrate.

Table II. Some Characteristics of Synthesized Nano TiO_2 and TiO_2 Nanocomposite Coatings

Crystalline structure	Samples	Absorption edges (nm)	Band gap energy (eV)	BET surface area (m^2/g)	Pore volume (cm^3/g)	XRD crystal size (nm)	TEM crystal size (nm)
Anatase, Rutile	Degussa	390	3.2	51	0.018	25	25–30
Anatase	TiO_2	400	3.1	350	0.125	8	5
Anatase	Ag-TiO_2	435	2.85	372	0.132	7	<5
Anatase	Zr-TiO_2	425	2.91	290	0.103	6	<5
Anatase	Ag-Zr-TiO_2	450	2.75	318	0.113	15	5–10

loss of the sample with the increase in temperature can be followed by thermogravimetrical analysis. The TGA analysis of the pure PAN fiber (Figure 8) can be roughly divided into three steps according to the extent of weight loss.[36] The first step is up to about 250°C, where weight loss is very small. It is inferred that there is only cyclization occurring in this step. The second step is up to about 300°C. During this step, the rate of weight loss becomes quite rapid, which is mainly due to the dehydrogenation. It is apparent that the weight loss of PAN/TiO_2 and PAN/TiO_2 nanocomposites is larger than that of PAN. It implies that TiO_2 and TiO_2 nanocomposites have promoted the dehydrogenation to some extent. In the last step, fragmentation of polymer chains occurs and producing volatile species leading to weight loss. After combustion of all organic part in TiO_2-modified fibers and doped-TiO_2 modified fibers, the residual amount corresponds to nanoparticles of TiO_2 and TiO_2 nanocomposites. As shown in Figure 8, a residual weight of about 6% wt has been obtained at 800°C for the pure fiber. The residual weights of about 11.5% wt, 17.5% wt, 20.3% wt, and 23.6% wt were obtained for TiO_2, Ag-TiO_2, Zr-TiO_2, and Ag-Zr-TiO_2 modified fibers with respect to residual weight of the pure fiber, respectively. These values are due to the TiO_2, Ag-TiO_2, Zr-TiO_2, and Ag-Zr-TiO_2 deposition onto the samples surface. From this result, it is evident that the thermogravimetric analysis technique in air allows evaluating the presence of TiO_2 and TiO_2 nanocomposites incorporated in the fibers.

Photocatalytic Self-Cleaning Activity

The photocatalytic activities (self-cleaning test) of the prepared TiO_2 nanocomposite/fibers were performed by observing the photodegradation oxidation of MB and Eosin Y dyes, which were preadsorbed on the untreated and treated fabrics. These dyes have strong adsorption characteristics on many surfaces, good resistance to light degradation, and well defined optical absorption maxima in the visible region. The dye method was used for evaluating the photocatalytic activity of self-cleaning samples. In the dye method, the whole process of the photodegradation of dyes under UV irradiation is monitored, and the performance of self-cleaning materials is evaluated with the aid of the discoloration of dyes.

The photocatalytic activity of our synthesized TiO_2 and TiO_2 nanocomposites on fibers were investigated by exposing the samples containing preadsorbed methylene blue and Eosin Y to UV–vis light. The photodegradation of MB and Eosin Y on the TiO_2 nanoparticles surface deposited on the fabrics was followed by dyes concentration changes (C/C_0) as a function of UV–vis illumination time.

All the TiO_2-coated samples possessed the ability to decompose dyes upon UV–vis irradiation. The UV–vis reflectance spectra of coated samples with dyes prior and after illumination were recorded. The absorption peaks, corresponding to the dyes, diminished under reaction which indicates that the dyes were degraded. No new absorption bands appear in the visible regions. The disappearance rate of the bands due to MB and Eosin Y adsorbed on the TiO_2-covered fibers is much higher than those observed for the untreated fibers [Figures 9(a, b) and 10(a, b)]. This is not unexpected since the photocatalytic activity of TiO_2 is well known. Also, irradiation of all the doped TiO_2-fibers samples show enhanced photocatalytic activities, comparing with the undoped TiO_2 coated fibers [Figures 9(c, d) and 10(c, d)]. The Zr-TiO_2 and Ag-TiO_2 samples exhibit a much higher efficiency in the degradation of dyes than pure TiO_2. In particular, Ag-Zr-TiO_2 shows the highest photocatalytic activity among all the samples [Figures 9(e) and 10(e)]. The photocatalytic activity of samples decreased in the following order: Ag and Zr co-doped TiO_2 > Ag-doped TiO_2 > Zr-doped TiO_2 > undoped TiO_2.

The photodegradation of organic dyes on the surface of a TiO_2-based photocatalyst is generally initiated by the irradiation of UV–vis light source, which excites and transitions the electrons from the valence band to the conduction band. Subsequently, these electrons are captured by the adsorbed O_2 to give $O_2^{\cdot -}$, and the water molecules adsorbed on the surface of the catalyst

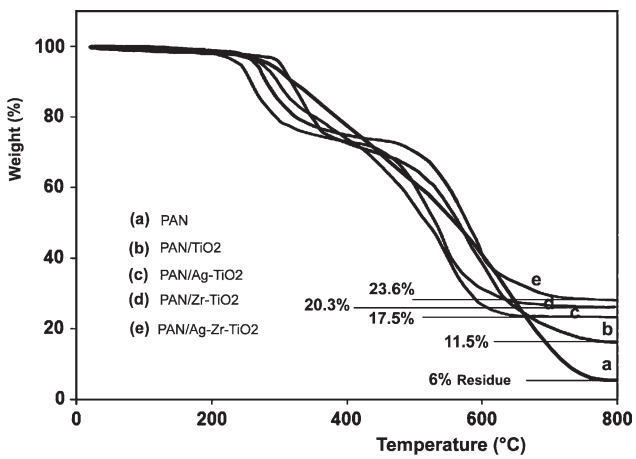

Figure 8. TGA analysis of pure PAN and PAN/TiO_2 nanocomposites.

Applied Polymer SCIENCE

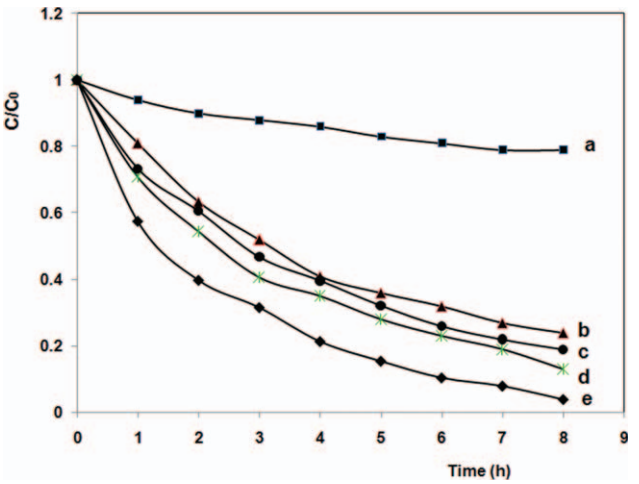

Figure 9. Photocatalytic decomposition rate of MB against irradiation time. (a) MB on untreated fiber, (b) MB on TiO_2 coated fiber, (c) MB on Zr-TiO_2 coated fiber, (d) MB on Ag-TiO_2 coated fiber, and (e) MB on Ag-Zr-TiO_2 coated fiber. (Experimental conditions: Temperature: 25°C, air pressure: 1 atm, UV–vis irritation source: 400 W high pressure mercury lamp). [Color figure can be viewed in the online issue, which is available at wileyonlinelibrary.com.]

react with the hole(+) vacancies to give OH·. Finally, these active oxygen species attack the dye molecules and decompose them. The proposed sequential mechanism is as follows.

(a) Absorption of energy

$$TiO_2 + h\nu \rightarrow h^+ + e^- \quad (1)$$

(b) Generation of active oxygen species

$$O_2 + e^- \rightarrow O_2^{\bullet} - \quad (2)$$

$$H_2O + h^+ \rightarrow H^+ + OH^{\bullet} \quad (3)$$

(c) Oxidation of dyes

$$\text{Dyes} + O_2^{\bullet} - \rightarrow \text{Degradation products} \quad (4)$$

$$\text{Dyes} + OH^{\bullet} \rightarrow \text{Degradation products} \quad (5)$$

In addition to the reasons mentioned above, dye photosensitized process might affect the photocatalytic activity. Dye sensitization facilitates electron transfer between the dye molecules and the host TiO_2. Various dyes such as methylene blue and Eosin Y have been used to sensitize TiO_2 nanoparticles.[56] These surface adsorbed dye molecules are excited upon illumination by UV–visible light and inject electrons into the conduction band of host semiconductor. This injection is favorable due to the more negative potential of the lowest unoccupied molecular orbital (LUMO) of the dye molecules as compared to the conduction band potential of TiO_2. The electrons injected by dye molecules hop over quickly to the surface of titania where they are scavenged by molecular oxygen to form superoxide radical $O_2{\cdot}^-$ and hydrogen peroxide radical ·OOH. These photoactive radicals decolorize and mineralize substrate dyes by destroying their chromophore structure.

It has been demonstrated that incorporating Zr^{4+} into TiO_2 can introduce lattice defects and lead to higher photoactivities than those of the pure oxide. The introduced defects not only reduce the band gaps, but also play a role as charge-trapping centers in inhibiting charge recombination. A few defects in a TiO_2 matrix, resulting from the presence of dopants, can play the role of trapping centers to inhibit charge recombination and improve the photoactivity.[14]

The mechanism of variation of photoactivity for Ag-TiO_2 coating can be explained as below. The size of TiO_2 particles in Ag-TiO_2 coating is similar to that in TiO_2 coating without Ag [Figure 6(a, b)]; thus the variation of photocatalytic activity cannot be ascribed to size effect. When two materials of different work functions get in contact, the Schottky barrier will be formed and electrons will transfer from the material with low work function to the material with high work function.[52] Silver and TiO_2 have different work functions and the work function of silver is higher than TiO_2 (work function $\Phi_{TiO2} = 4.2$ eV, $\Phi_{Ag} = 4.6$ eV). So when silver contacts with TiO_2, electrons will transfer from TiO_2 to silver. Those electrons transferred to silver and loaded on the surface of silver will be scavenged by the electron acceptor, commonly the oxygen molecules absorbed on the surface of silver. Meanwhile, some electrons transferred to silver are contained in the body of TiO_2. Though there was no electron scavenger, the transfer decreases the recombination between electron and hole. Whether in body or on the surface of silver, silver atoms act as electron traps that capture certain amount of photoelectrons produced by UV excitation and increase the separation between photoelectron and hole. Thus more holes will have the opportunity to escape from the geminate hole–electron recombination. It is well known that the geminate recombination is the main reason for low efficiency of TiO_2 photocatalysis. Therefore, the existence of silver atom in Ag-TiO_2 coating can help more holes to

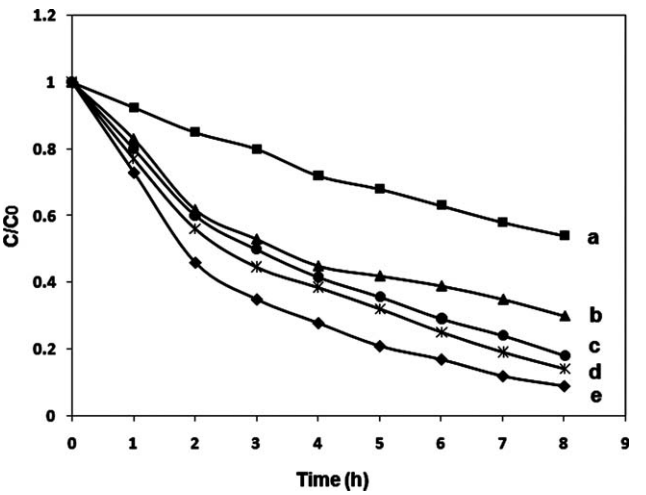

Figure 10. Photocatalytic decomposition rate of EY against irradiation time: (a) EY on untreated fiber, (b) EY on TiO_2 coated fiber, (c) EY on Zr-TiO_2 coated fiber, (d) EY on Ag-TiO_2 coated fiber, and (e) EY on Ag-Zr-TiO_2 coated fiber. (Experimental conditions: Temperature: 25°C, air pressure: 1 atm, UV–vis irritation source: 400 W high pressure mercury lamp).

transport to the surface and enhance the photocatalytic efficiency.[57]

The co-doped (Ag–Zr) TiO_2 exhibits highest photocatalytic activity, which is believed to be due to the enhanced light absorption resulting from the narrowing of the band gap and synergistic effect between the Ag and Zr doped into TiO_2 lattice. When both Ag and Zr are involved as co-doped in the nanocrystalline TiO_2 particles, a cooperative action ensues. Silver doped or deposited on TiO_2 are expected to show various effects on the photocatalytic activity of TiO_2 by different mechanisms. This noble metal may act separately (i) enhance the electron–hole separation by acting as electron traps, (ii) extend the light absorption into the visible range and enhance surface electron excitation by plasmon resonances, and (iii) modify the surface properties of photocatalysts. Also Zr-doping induced the increase of the photocatalytic efficiency. On the one hand, Zr doping into the TiO_2 lattice results in relatively larger lattice strain. To balance this strain, lattice oxygen, especially surface oxygen atom can escape from the lattice and exist as a hole trap. Also Zr-doping introduces a few defects into a TiO_2 matrix, it is preferential for electrons to be trapped on Zr^{4+} than on $Ti^{4+,}$ these defects can play the role of trapping centers to inhibit charge recombination and improve the photoactivity.[58] So the photocatalytic activity of co-doped TiO_2 is markedly improved.

Finally, a strong Ag–Zr synergistic interaction appears to play a decisive role in driving the excellent photoactivity performance of Ag–Zr co-doped materials by affecting (i) electronic properties, particularly highest decrease of the anatase band gap and subsequently enhancing the visible light photon absorption, and (ii) surface properties, which is related to the formation of active radicals upon light irradiation.

CONCLUSION

Titania and titania nanocomposites (doped by Ag, Zr, and Ag-Zr) were coated on PAN fibers via sol–gel dip-coating method. Modified PAN fabrics with deposited TiO_2 nanoparticles and TiO_2 doped and co-doped nanocomposite exhibited outstanding self-cleaning activity. Photocatalytic self-cleaning potential of the prepared nanocomposites was assessed by photodegradation of MB and EY under UV–vis light. The materials showed photocatalytic activity originated from TiO_2, doped and co-doped TiO_2 on their surface. A pronounced enhancement of photocatalytic activity was observed for all doped and co-doped samples. The small particles size and high surface area are assisting for the observed enhanced photoactivity. In the photodecomposition of MB and EY, Ag–Zr co-doped TiO_2 coated fiber showed the highest photocatalytic efficiency as compared to that of pure TiO_2 and mono- doped TiO_2 nanocomposites. The enhanced photoactivity of the co-doped Ag–Zr TiO_2-coted fibers is believed to be due to the synergistic effect between the Ag and Zr doped into TiO_2 lattice and enhanced light absorption resulting from the narrowing of the band gap. Such strong effect supposed to be related to effective inhabitation of the recombination of photogenerated electrons and holes and creation of an increased concentration of active radical species.

ACKNOWLEDGMENTS

The authors are grateful to University of Guilan for financial assistance of this research project.

REFERENCES

1. Sarria, V.; Deront, M.; Péringer, P.; Pulgarin, C. *Appl. Catal. B* **2003,** *40*, 231.
2. Yamashita, H.; Harada, M.; Misaka, J.; Takeuchi, M.; Ikeue, K.; Anpo, M. J. *Photochem. Photobiol. A* **2002,** *148*, 257.
3. Giraldo, A. L.; Penuela, G. A.; Torres-Palma, R. A.; Pino, N. J.; Palominos, R. A.; Mansilla, H. D. *Water Res.* **2010,** *44*, 5158.
4. Fujishima, A.; Rao, T. N.; Tryk, D. A. *J. Photochem. Photobiol. C* **2000,** *1*, 1.
5. Hussain, M.; Ceccarelli, R.; Marchisio, D. L.; Fino, D.; Russo, N.; Geobaldo, F. *Chem. Eng. J.* **2010,** *157*, 45.
6. Wu, P. X.; Tang, J. W.; Dang, Z. *Mater. Chem. Phys.* **2007,** *103*, 264.
7. Wang, J. W.; Zhu, W.; Zhang, Y. Q.; Liu, S. X. *J. Phys. Chem. C* **2007,** *111*, 1010.
8. Fang. J.; Bi, X.; Si, D.; Jiang, Z.; Huang, W. *Appl. Surf. Sci.* **2007,** *253*, 8952.
9. Liu, Z. L.; Guo, B.; Liang, H.; Jiang, H. X. *J. Phys. Chem. Solids* **2005,** *66*, 161.
10. Xue, Y. H.; Zeng, Z. X. *J. Mol. Catal. A* **2008,** *279*, 77.
11. Zhou, G.; Raymond, J. H.; Gorte, J. *Appl. Catal. A* **2008,** *335*, 153.
12. Ismail, A. A.; Matsunaga, H. *Chem. Phys. Lett.* **2007,** *447*, 74.
13. Venkatachalam, N.; Palanichamy, M.; Murugesan, V. J. *Mol. Catal. A* **2007,** *273*, 177.
14. Chang, S.; Doong, R. J. *Phys. Chem. B* **2006,** *110*, 20808.
15. Gao, B.; Lim, T. M.; Subagio, D. P.; Lim, T. A. *Appl. Catal. A* **2010,** *375*, 107.
16. Zhao, G.; Kozuka, H.; Yoko, T. *Thin Solid Films* **1996,** *277*, 147.
17. Hilal, H. S.; Majjad, L. Z.; Zaatar, N.; El-Hamouz, A. *Solid State Sci.* **2007,** *9*, 9.
18. Liu, H. M.; Yang, W. S.; Ma, Y.; Yao, J. N. *Appl. Catal. A* **2006,** *299*, 218.
19. Sobana, N.; Muruganadham, M.; Swaminathan, M. J. *Mol. Catal. A* **2006,** *258*, 124.
20. Subramanian, V.; Wolf, E.; Kamat, P. J. *Phys. Chem. B* **2001,** *105*, 11439.
21. Dobosz, A.; Sobczynski, A. *Water Res.* **2003,** *37*, 1489.
22. Hufschmidt, D.; Bahnemann, D.; Testa, J. J.; Emilio, C. A.; Litter, M. I. *J. Photochem. Photobiol. A* **2002,** *148*, 223.
23. Shen, X. Z.; Liu, Z. C.; Xie, S. M.; Guo, J. J. *Hazard. Mater.* **2009,** *162*, 1193.
24. Yuan, Z. H.; Jia, J. H.; Zhang, L. D. *Mater. Chem. Phys.* **2002,** *73*, 323.
25. Lin, L.; Zheng, R. Y.; Xie, J. L.; Zhu, Y. X.; Xie, Y. C. *Appl. Catal. B* **2007,** *76*, 196.

26. Balek, V.; Li, D.; Subrt, J.; Vecernıkova, E.; Hishita, S.; Mitsuhashi, T.; Haneda, H. J. *Phys. Chem. Solids* **2007,** *68*, 770.
27. Ling, Q. C.; Sun, J. Z.; Zhou, Q. Y. *Appl. Surf. Sci.* **2008,** *254*, 3236.
28. Xua, Q.; Welliaa, D. V.; Ska, M. A.; Lima, K. H.; Loob, J.S. C.; Liaoc, D. W.; Amald, R.; Tan, T. T. Y. *J. Photochem. Photobiol. A* **2010,** *210*, 181.
29. Xu, J. H.; Li, J.; Dai, W. L.; Cao, Y.; Li, H.; Fan, K. *Appl. Catal. B* **2008,** *79*, 72.
30. Li, D.; Haneda, H.; Hishita, S.; Ohashi, N. *Chem. Mater.* **2005,** *17*, 2588.
31. Liu, G.; Zhao, Y.; Sun, C.; Li, F.; Lu, G. Q.; Cheng, H. M. *Angew. Chem. Int. Ed.* **2008,** *47*, 4516.
32. Yang, X.; Cao, C.; Erickson, L.; Hohn, K.; Maghirang, R.; Klabunde, K. J. *Catal.* **2008,** *260*, 128.
33. Valentin, C. D.; Finazzi, E.; Pacchioni, G. *Chem. Mater.* **2008,** *20*, 3706.
34. Mihailovic, D.; Šaponjic, Z.; Radoicic, M.; Radetic, T.; Jovancic. P.; Nedeljkovic. J.; Radetic, M. *Carbohydr. Polym.* **2010,** *79*, 526.
35. Moafi, H. F.; Shojaie, A. F.; Zanjanchi, M. A. *Appl. Surf. Sci.* **2010,** *256*, 4310.
36. Moafi, H. F.; Shojaie, A. F.; Zanjanchi, M. A. *J. Appl. Polym. Sci.* **2010,** *118*, 2062.
37. Moafi, H. F.; Shojaie, A. F.; Zanjanchi, M. A. *Thin Solid Films* **2011,** *519*, 3641.
38. Moafi, H. F.; Shojaie, A. F.; Zanjanchi, M. A. *J. Appl. Polym. Sci.* **2011,** *121*, 3641.
39. Bozzi, A.; Yuranova, T.; Guasaquillo, I.; Laub, D.; Kiwi, J. J. *Photochem. Photobiol. A* **2005,** *174*, 156.
40. Daoud, W. A.; Leung, S. K.; Tung W. S.; Xin, J. H.; Cheuk, K.; Qi, K. *Chem. Mater.* **2008,** *20*, 1242.
41. Dong, Y.; Bai, Z.; Zhang, L.; Liu, R.; Zhu, T. J. *Appl. Polym. Sci.* **2006,** *99*, 286.
42. Liuxue, Z.; Xiulian, W.; Peng, L.; Zhixing, S. *Surf. Coat. Technol.* **2007,** *201*, 7601.
43. Qi, K.; Xin, J. H.; Daoud, W. A.; Mak, C. L. *Int. J. Appl. Ceram. Technol.* **2007,** *4*, 554.
44. Xin, J. H.; Daoud, W. A.; Kong, Y. Y. *Text. Res. J.*, **2004,** *74*, 97.
45. Yuranova, T.; Laub, D.; Kiwi, J. *Catal. Today* **2007,** *122*, 109.
46. Tung, W. S.; Daoud, W. A. *Acta Biomater.* **2009,** *5*, 50.
47. Wu, D.; Long. M.; Zhou, J.; Cai, W.; Zhu, X.; Chen, C.; Wu, Y. *Surf. Coat. Technol.* **2009,** *203*, 3728.
48. Mejía, M. I.; Marín, J. M.; Restrepo, G.; Pulgarín, C.; Mielczarski, E.; Mielczarski, J.; Arroyo, Y.; Lavanchy, J. C.; Kiwi, J. *Appl. Catal. B* **2009,** *91*, 481.
49. Uddin, M. J.; Cesano, F.; Bonino, F.; Bordiga, S.; Spoto, G.; Scarano, D.; et al. *J. Photochem. Photobiol. A* **2007,** *189*, 2860..
50. Uddin, M. J.; Cesano, F.; Scarano, D.; Bonino, F.; Agostini, G.; Bordiga, S.; et al. *J. Photochem. Photobiol. A* **2008,** *199*, 64.
51. Yang, J.-H.; Han, Y.-S.; Choy, J.-H. *Thin Solid Films* **2006,** *495*, 266.
52. Sánchez-Soto, P. J.; Avilés, M. A.; del Ŕio, J. C.; Ginés, J. M.; Pascual, J.; Pérez-Rodŕiguez, J. L. *J. Anal. Appl. Pyrol.* **2001,** *58*, 155.
53. Dongfeng, S.; Dawei, G.; Qufu, W.; Lizhen, T.; Hong, Z.; Mingqiao, G. *Fibers Polym.* **2011,** *12*, 214.
54. Grandcolas, M.; Du, M.K. L.; Louvet, F.B. A.; Keller, N.; Keller, V. *Catal. Lett.* **2008,** *123*, 65.
55. Hikmet, S. *Appl. Catal. A* **2007,** *319*, 230.
56. Shama, R.; Ruh, U.; Butt, A. M.; Gohar, N. D. *J. Hazard. Mater.* **2009,** *70*, 560.
57. Houa, X.; Huanga, M.; Wub, X.; Liub, A. *Chem. Eng. J.* **2009,** *146*, 42.
58. Haijin, L.; Guoguang, L.; Qingxiang, Z. J. *Solid State Chem.* **2009,** *182*, 3238.